Hybrid electric distributed propulsion overall aircraft design process and models for general aviation (FAST GA)

J P Ruscio[1], J Jezegou[1], E Benard[1], A Gomez Pacheco[1], P Laonet[1] and R Alonso Castilla[1]

[1] ISAE-SUPAERO, Université de Toulouse, France

Corresponding author: juan.ruscio@isae-supaero.fr

Abstract. In the frame of the European objectives in terms of CO2 emissions, the aeronautics is looking for a technological rupture to achieve them, in particular, the aircraft design domain pursuits this through the research of innovative architectures. One of these innovative configurations currently being explored includes the hybrid electric energy source (thermal/electric) for Distributed Electric Propulsion (DEP) architecture. This Paper details a code developed to size a general aviation aircraft at concept level, by only defining its top level requirements and the main architecture parameters. The code can manage both conventional and hybrid power source as well as concentred or distributed propulsion architectures in order to allow the user to evaluate and compare the feasibility and benefits respectively of these innovative architectures. This code is a branch of the code "FAST-CS25" (Future Aircraft Sizing Tool for conventional CS-25 type) held by ONERA/ISAE-SUPAERO. The presented work aims at the expansion of the FAST code to CS-23 conventional type, hybrid electric energy source, and distributed propulsion system configurations. Through this paper, the models and the main sizing loops for the concept design are described, but putting special emphasis on the distributed propulsion aerodynamics and wing mass estimation. These detailed models where validated with the NASA X-57 DEP aircraft satisfactory. The whole concept design loop of a hybrid energy aircraft was validated with the eGenius hybrid energy aircraft.

1. FAST GA development

FAST GA stands for "Future Aircraft Sizing Tool for Genaral Aviation", it is divided in 3 main options: a) Conventional aircraft, b) Hybrid energy aircraft, and c) Hybrid energy DEP aircraft. The main objective of the code is to size an aircraft at concept level of any of the 3 configurations above mentioned given the TLAR, and both, technological and design choices. Even though the models and many design logics where changed and reviewed from the legacy FAST-CS25 type [1], the main outline of the code organization for the conventional configuration is mainly the one showed in [1].

In FAST GA for conventional aircraft, the models for geometry, mass breakdown (except for the wing mass explained in Section 2), performance and aerodynamics are mainly taken from [3], [5], [8], and [9], some details regarding own aerodynamics model choices and developments for conventional configuration are explained in Section 3.

More elaborated models were developed for the DEP aerodynamics effects as explained in Section 4. And finally, energy hybridization models, and its sizing logics are explained in Section 5. The main code modules, information flow and loops are shown in figure 1, the modules and loops with star (*) are the ones that were developed for the Hybrid energy configuration option exclusively.

The conventional configuration option of FAST GA was benchmarked successfully with the Beechcraft 76 aircraft with less than 5% error in mass, geometry, take-off field, and fuel consumption with a design mission of 12.000 ft. and 151 KTAS cruise altitude and speed respectively, a range of 780NM and payload of 395 Kg. The validation for the hybrid energy option is detailed in Section 5.

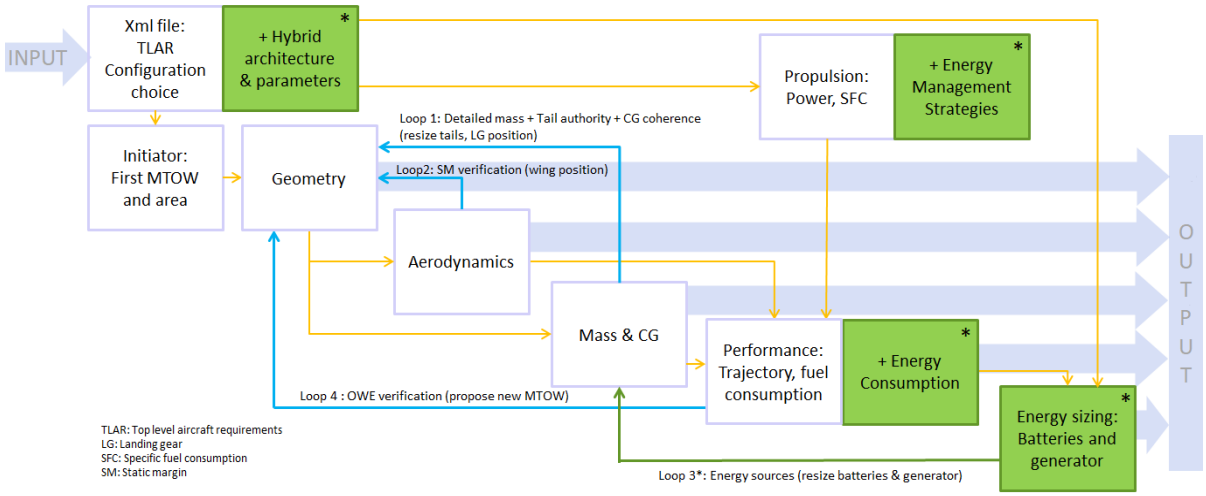

Figure 1. FAST GA modules and main sizing loops logic (* for hybrid configuration).

2. Wing mass model for DEP

Firstly, only statistical models have been used in FAST GA to predict the mass of the wing, but the addition of new features to the design, such as hybrid/electric distributed propulsion, makes it useless and inaccurate. As a result, a detailed semi-analytical methodology has been developed to predict the structural mass of the wing following the strength requirements in the CS-23.

2.1. Methodology

Regarding the model, the wing is assumed to be trapezoidal, with N engines distributed along the span and divided into a primary and a secondary structure. The primary structure is modeled as a wing-box composed of three structural elements (the main spar with I-section composed of two flanges and a web, the skin and the ribs) and a miscellaneous or non-optimum weight to account the joints, cut-outs, connections, etc. Moreover, it is assumed that each of these components is designed to support, exclusively, one type of solicitation: the spar web withstands the shear force, the spar flanges support the bending moment and the skin reacts the torsion moment. This hypothesis, allows a simplified analytical estimation of their individual mass, based on É. Roux's model [2]. For the computations it is considered an elliptical distribution of the lift and the weight, including both the wing and the fuel mass, as well as the punctual weight and trust of each engine which induces a great alleviation effect on the bending moment. Then, the stress constraint ruled by certification requirements is applied in and within the boundaries of the flight envelope, with the corresponding factor of safety, geometry and material inputs. On the other hand, Torenbeek [3] states that the secondary structure (ailerons, flaps, slats…) contributes around a 25% to the total mass of the wing. Thus, its weight will be empirically obtained with this proportion.

In addition to the previous model, an advanced version has been developed for the latest aircraft designs. Sui An [4] shows in her studies the impact of flutter on the wing mass when using distributed propulsion and proves that the flutter constraint increases the optimum mass a 6-14 %. However, the use of composite materials in general aviation allows lightening the structure a 10-15 % attending to Raymer's statistics [5]. Therefore, the new model will approximate such effects in the applicable cases through a mean coefficient: 1.10 for flutter in DEP aircraft and 0.875 for composite materials when no technical data is available about them.

2.2. Validation

The validation of the model is performed for two aircraft: the conventional double-engine Beechcraft 76 and the innovative X-57 Maxwell with DEP. In both cases it has been compared the statistical estimation of Raymer with the developed semi-analytical approach. The results in table 1 confirm the accuracy of the semi-analytical model for conventional aircraft designs with an extremely low error of 0.3 % with respect to the statistical value. The next step is to prove that the model is flexible enough to adapt to the new trends, and in particular to DEP airplanes. Effectively, the semi-analytical advanced model provides an optimum wing mass for the X-57 with a deviation of 0.7 % from the reference value [6] and of 4.6 % without considering the empirical coefficients of flutter and composites. Still, the semi-analytical model provides higher accuracy than the statistical one, which fails on the estimation of the wing mass for innovative designs.

Table 1. Comparisons of different wing mass models for innovative and conventional aircrafts.

	Beechcraft 76		X-57 Maxwell	
	Wing mass [Kg]	Error [%]	Wing mass [Kg]	Error [%]
Semi-analytical	192.4	0.3	174.4	4.6
Semi-analytical advanced	-	-	167.8	0.7
Statistical	191.8	REFERENCE	126.8	23.9
Reference value [6]	-	-	166.7	REFERENCE

3. Conventional aerodynamics model

Legacy FAST-CS25 [1] models were reviewed and adapted to GA aircraft. An important development was *FastVLM*, a Vortex Lattice wing solver written in Python. It provides the lift distribution and induced drag in a faster and more integrated way. It was validated against AVL [7], also with flaps.

3.1. Drag polar

A simple parabolic model was implemented. Parasitic drag is calculated using a component build-up method (flat plate analogy, with empirical form FF and interference IF factors taken from [8]). Miscellaneous drag contributions are included in $C_{DOother}$. The Oswald factor comes from *FastVLM*.

$$C_D = C_{D0} + C_{Di} = \frac{1}{S_{ref}} \sum c_{fi}\, FF_i\, IF_i\, S_{wet\,i} + C_{D0\,other} + \frac{1}{\pi A e} C_L^2 \tag{1}$$

Drag results are compared against data from Daher TBM 940, and from Roskam [9] of Cessna 310 and SAAB 340 aircraft. The obtained precision was satisfactory for preliminary design.

3.2. Lift curve

The lift curve of the complete aircraft is approximated by that of the wing alone. For flap deflections, Roskam empirical methods [9] were chosen over *FastVLM* to account for different flap types.

The stalling point is calculated using *xFoil* [10] to get the C_{Lmax} of the root and tip airfoils, and the lift distribution from *FastVLM* to achieve a more accurate result of C_{Lmax} and of where the stall begins.

3.3. Calculations of the horizontal tail

The lift coefficient at the horizontal tail and its derivative are needed for stability calculations, and in its sizing method. *VSPAero* [11] is used here as it accounts for the effect of wing downwash.

4. DEP aerodynamics model

A new model was developed to calculate the aerodynamic effects of DEP. It is simple and computationally cheap, which makes it ideal for FAST GA. It is based on Patterson's work [12].

4.1. Lift increment

The core is the bidimensional lift increment caused by propeller slipstream. Two effects are considered: the variation of the effective angle of attack, and the dynamic pressure increase. It is calculated in equation (2) (which was derived for a symmetrical airfoil). The definition of the angles (propeller incidence and angle of attack) is shown in figure 2. Unlike in [12], α_g is set with respect to the zero-lift line of the airfoil (accounting for high camber or flaps). Vp is the velocity induced by the propeller, which is added vectorially to V_∞, it is obtained using momentum theory, which is useful as it only depends on the thrust coefficient ($Tc = T\,(\rho V^2 D^2)^{-1}$). Finally, β is a reduction factor to account for the finite slipstream height, taken from a surrogate model in [12].

$$\left.\frac{\Delta L}{L_0}\right|_{2D} = \left(1 - \frac{\beta V_p \sin i_p}{V_\infty \sin \alpha_g}\right)\sqrt{1 + 2\frac{\beta V_p}{V_\infty}\cos(\alpha_g + i_p) + \left(\frac{\beta V_p}{V_\infty}\right)^2} - 1 \tag{2}$$

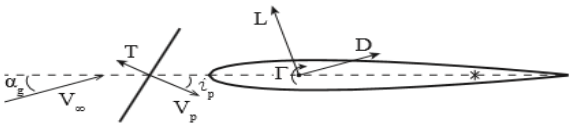

Figure 2. Scheme of the airfoil lift increment and angle definitions from [12].

This result is extrapolated to estimate the wing lift variation as equation (3). For each rotor it takes the local lift coefficient from the VLM code, to account for lift asymmetries like the flap deployment. Other simplifications are a constant V_p along the chord, no stall, and no effect of tangential velocity.

$$\Delta C_L = \sum_{i=1}^{n_{rotors}} (\Delta C_L)_{i_{2D}} \left(\frac{S_{blown}}{S_{ref}}\right)_i \tag{3}$$

To compute the new C_{Lmax}, it was assumed that the stalling angle remains constant. This is not true, but the complexity of the flow makes it difficult to define a new stalling point. The fact that it is conservative to leave the maximum angle unchanged leaded us to proceed this way.

4.2. Drag increment

Equation (4) shows the drag increment, which follows the same parabolic model as the conventional FAST GA. There are three variations with respect to the unblown case:

- $\Delta C_L{}^2$. The most important term, as lift increment are very high.
- Oswald factor (e). In general, propeller action degrades the spanwise lift distribution, decreasing e. A parabolic evolution of e with respect to V_p was included. This approach was suggested in [12] based on VSPAero [11] simulations.
- ΔC_{D0}. Velocity growth on the wing increases friction. This effect was included is small.

$$\Delta C_D = \Delta C_{D_0} + \frac{1}{\pi A e'}(C_L + \Delta C_L)^2 - \frac{1}{\pi A e} C_L^2 \tag{4}$$

An additional factor can modify the Oswald factor e, a properly designed wingtip engine can interact with the wingtip vortex and improve the efficiency, this is added as technological factor option

4.3. Pitching moment

As the C_m is computed at the wing aerodynamic centre, the main effect of DEP will be the dynamic pressure increment, this increases the unblown coefficient, equation (5). The effect of the propeller normal force was estimated, but it is much smaller.

$$\Delta C_m = \sum_{i=1}^{n_{rotors}} \frac{\Delta q}{q_\infty} \frac{S_{blown_i}}{S_{ref}} \frac{\bar{c}_i}{\bar{c}} C_{m_0} \tag{5}$$

4.4. Validation of the model

Three test cases were analysed: a CFD simulation of the NASA X-57 [13], and two wind tunnel tests [14] and [15]. Only the first analysis is presented, as it resembles more our desired configuration. It corresponds with a landing phase, with a 40º flap deflection and high thrust on DEP rotors (Tc=0,611). In table 2, the figures of "Un-blown" and "Δblow CFD" are the results from CFD simulations of the wing with no thrust and the variation induced to the coefficients by the thrust ON respectively taken from [13]. Then, "Δblow Model" are the results of the variation induced by the thrust from FAST GA model described in this paper; finally, the "error" column shows the comparison of the final coefficients results for the blown case of FAST GA model with respect to the blown case from [13].

Table 2. Validation results of DEP model (un-blown and Δblow-CFD data from [13]).

	Cl				**Cd**				**Cm**			
AoA (º)	Un-blown	Δblow Model	Δblow CFD	Error (%)	Un-blown	Δblow Model	Δblow CFD	Error (%)	Un-blown	Δblow Model	Δblow CFD	Error (%)
0	1.68	3.00	2.88	4.17	0.11	0.31	0.32	-3.1	-0.40	-0.79	-0.82	-3.7
2	1.87	3.28	3.21	2.2	0.12	0.35	0.38	-7.9	-0.40	-0.78	-0.82	-4.9
4	2.05	3.56	3.54	0.6	0.14	0.41	0.44	-6.8	-0.39	-0.76	-0.81	-6.2
6	2.24	3.83	3.83	0.1	0.16	0.47	0.50	-6.0	-0.38	-0.73	-0.79	-7.6
8	2.42	4.11	4.18	-1.7	0.19	0.54	0.63	-14.3	-0.38	-0.72	-0.78	-7.7

The results are in general within the conceptual design tolerances, even though the wing has a high camber and flap deflections. The model is therefore validated for the current purpose of FAST GA.

4.5. Implementation in FAST GA

The DEP methods calculate the increments of lift and drag. These depend on the flight condition (V, AoA) and the power for each high lift engine. There are two possibilities:

- Known C_L (V2 speed, climb). There is a nonlinear relation between AoA and the lift caused by DEP, while the total C_L is imposed. AoA is then solved iteratively. An additional iteration was added for the optimal climbing calibrated speed, as the the DEP action modifies the L/D ratio.
- Known AoA (Takeoff). Here, C_L and ΔC_L are computed directly.

DEP can be conceived as a high lift system, and it would be optimal to have it retracted during cruise relying in wingtip propellers, this is the default configuration, but FAST GA is prepared to include others, like using the distributed engines as the only source of thrust.

5. FAST GA for hybrid-electric aircraft sizing

This section deals with the adaptation of FAST GA to hybrid electric aircrafts and will develop the models of the powertrain, the sizing of the energy sources and the results obtained on a test case for Series Hybrid architecture.

5.1. Powertrain

The objective of the powertrain developed in this study is to be generic, meaning that any standard hybrid architectures (parallel, series, turboelectric…) could be modelled by this single powertrain skeleton. A diagram is presented in figure 3.

- On the left, the thermal engine can be chosen to be an Internal Combustion Engine (ICE) or a Gas Turbine (GT) by the designer.
- Then on the right, there are the mechanical components, plus the gearbox in the centre (but it was neglected here due to the focus made on Series Hybrid in the rest of the study).
- Finally, the rest represents the whole electrical chain, simplified to its core elements (Electric Motor (EM), Converter, Battery & other components modelled by one efficiency) with

numerous first approximation assumptions: no electrical off-takes (for powering avionics for instance) or voltage considerations, and the battery is equivalent to 'energy in a box' (no cell architecture or voltage).

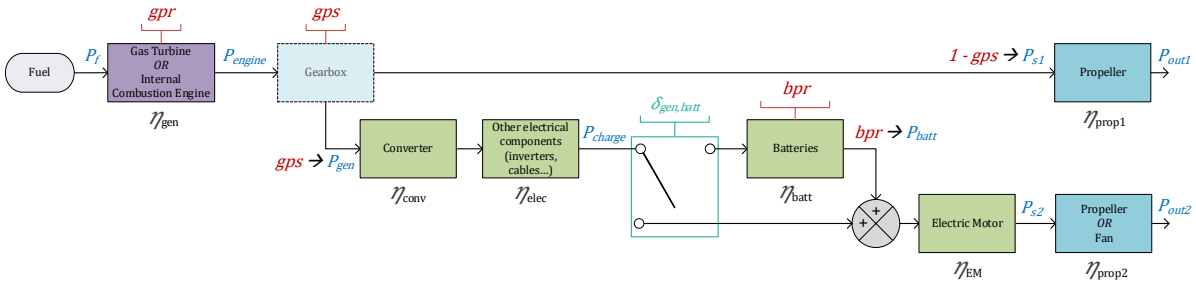

Figure 3. Powertrain skeleton.

After the components diagram is established, some control parameters are required and adapted from [16]. Some are real-time parameters which can vary during the mission analysis while others are fixed for the whole design process. On top of the control parameters, we use 2 additional parameters adapted from [16] & [17] to link the energy sources, the input and output Degree of Hybridization (DoH). All parameters are summed up in table 3.

Table 3. Powertrain parameters.

	Parameter		Description	Usage
Control	$\delta_{gen,\,Batt}$	$= \begin{cases} 0 \Rightarrow \text{no battery recharge} \\ 1 \Rightarrow \text{battery can be charged} \end{cases}$	Determine if the batteries can be charged or not	fixed
	gpr	$gpr(t) = \frac{P_{engine}(t)}{P_{engine,max}} \in [0,1]$ [1]	Generator Power Rate (~ generator throttle)	real-time
	bpr	$bpr(t) = \frac{P_{Batt}(t)}{P_{Batt,max}} \in [0,1]$ [1]	Battery Power Rate (~ 'electric' throttle)	real-time
	gps	$gps(t) = \frac{P_{gen}(t)}{P_{engine}(t)} \in [0,1]$ [1]	Generator Power Share, ratio of generator power converted to electric power	real-time
Hybrid	Φ_{in} [2]	$= \frac{P_{Batt,\,max}}{P_{Batt,\,max} + P_{engine,\,max}}$	Input Degree of Hybridization, ratio of maximum electrical power onboard with total max power	fixed
	ϕ_{out} [1]	$\phi_{out}(t) = \frac{P_{s2}(t)}{P_{s2}(t) + P_{s1}(t)}$	Output Degree of Hybridization, ratio of output shaft power from EM onboard with total output shaft power	real-time

[1] Adapted from [16]
[2] Adapted from [17]

The link between the hybrid architectures previously mentioned and the control parameters is depicted in table 4. Indeed, the first 'parameter' chosen by the designer in the process is the architecture he wants to size, and this decision fixes some of the powertrain parameters. All other unfixed parameters then become design variables (the '*' in table 4). A high number of variables means a more complex architecture but consequently more freedom left to the designer.

Table 4. Link between hybrid architectures and powertrain parameters.

Architecture	Φ_{in}	ϕ_{out}	$\delta_{gen,\,Batt}$	gps
Parallel Hybrid	*	*	0	$0\ \forall t$
Series Hybrid	*	$1\ \forall t$	1	$1\ \forall t$
Series-Parallel partial Hybrid	*	*	1	*
Full Turboelectric	0	$1\ \forall t$	0	$1\ \forall t$
Partial Turboelectric	0	*	0	*

5.2. Mission analysis & Energy sources sizing loop

When the powertrain model is complete and integrated in the code, the second part of the study is about the mission analysis module adaptation and the hybrid energy sources sizing.

Starting from here the study is focused only on a Series Hybrid architecture. Thus, for the designer, the variables are: the architecture (Series here) and the input DoH Φ_{in} (used here to fix the generator max power with regard to the battery max power).

As outlined in [17] the sizing of hybrid energy sources can only rely on a time step mission analysis computation. This is required to compute both the total energy consumed by the EM and the total energy generated by the generator. These energies are computed by time step integration during the whole mission, taking into account the power used to charge the batteries at each time step.

The main parameter used to assess the progress of the energy sources sizing and to control the charging strategy is the battery State Of Charge (SOC), mainly because it links both the energy consumed, the energy generated and the battery energy capacity through the following relationship, where $E_X(t)$ corresponds to the energy consumed (resp. generated) until the point t (time).

$$SOC(t)=SOC_{initial}-\frac{E_{consumed}(t)-E_{generated}(t)}{E_{Battery,Max}} \quad (6)$$

Regarding the charging strategy, is kept very simple and could be upgraded to more refined level: if SOC reaches 100%, turn the generator OFF and if it falls below 70%, turn the generator back ON.

The sizing loop that is added to all the other sizing loops runs at fixed geometry, and thus fixed mass breakdown and aerodynamics as shown in figure 1. It loops on the mission analysis until the battery SOC stays between 100% and a low-limit SOC_{min} (usually 20%) at any point of the flight. The generator power is then fixed by the input DoH and updated at each iteration. When the loop finally converges, the process goes back to a geometry & mass breakdown computation to take into account the new battery & generator masses. The hybrid aircraft finally converges when the two following conditions are fulfilled: OWE converged and energy sources converged. This energy sizing loop can probably be optimized in the next versions of the code.

5.3. Test case

The resulting code adapted for hybrid electric aircraft is finally tested on TLARS of an existing aircraft to compare the obtained results with real aircraft data. The test case chosen is the eGenius Series Hybrid Aircraft from IFB Stuttgart whose data can be found in [18] (Hybrid, but not DEP case). The results obtained are very promising for the mission: 300 NM @6500ft (+30 min reserve @3000ft)

Table 5. Resulting figures of the FAST GA for hybrid energy aircraft design.

Disciplinary field	Description	Relative error with eGenius in [18]
Geometry	Wing area, Wingspan, Fuselage length	< 2%
Masses	MTOW, OWE	< 7%
Energy Sources	Battery mass, Generator max power	< 4%
Fuel consumed	by the generator	15.8% more

It is worth to note that even though the fuel consumed is a bit superior to the real aircraft's (19.7 kg output of FAST GA, 17kg for the eGenius in [18]), the benefits of hybridization are still visible compared to the conventional aircraft taken as example in [18], the Valentin Taifun II, which consumes 37kg for the same mission.

6. Conclusions and future work

FAST GA for conventional configuration, hybrid energy, and hybrid energy DEP has been successfully deployed. The code was successfully validated in the conventional and hybrid energy options. A validation in the hybrid energy DEP option is yet to be done due to the lack of a real existing case data, nevertheless the DEP aerodynamics model has been validated itself as shown in Section 4.

FAST GA is currently being transferred to an open source version in FAST-OAD [19] architecture which is the new generation of concept aircraft design tool developed by ONERA/ISAE-SUPAERO that relies in the OpenMDAO frame for better modularity, solver efficiency and the feature of MDO.

Acknowledgments
The authors would like to express their gratitude to the airplane manufacturer Daher for providing means to support the work presented in this paper through the research chair ISAAR « Innovative Solutions for Aviation Architecture & Regulation ».

References

[1] Schmollgruber P, Bartoli N, Bedouet J, Defoort S, Gourinat Y, Benard E, Lafage R, Sgueglia A. 2017 Use of a certification constraints module for aircraft design activities. In*17th AIAA Aviation Technology, Integration, and Operations Conference* (p. 3762)
[2] Roux É 2006 *Modèle de masse voilure, avions de transport civil (Pour une approche analytique de la dinamique du vol* vol 2) Doctoral dissertation (Toulouse: SUPAÉRO and ONÉRA)
[3] Torenbeek E 1992 *Development and application of a comprehensive, design-sensitive weight prediction method for wing structures of transport category aircraft* Report LR-693 (Delft: Delft University of Technology-Faculty of Aerospace Engineering) p 16
[4] An S 2015 *Aeroeslasticc design of a lightweight distributed electric propulsion aircraft with flutter and strenth requirements* Doctoral dissertation (Atlanta: Georgia Institute of Technology-School of Aerospace Engineering) p 48
[5] Raymer D P 2018 *Aircraft design: a conceptual approach* (Reston, VA: American Institute of Aeronautics and Astronautics, Inc) ed J A Schetz p 580
[6] Moore M D 2016 *Distributed electric propulsion (DEP) aircraft* 5th Symposium on Collaboration in Aircraft Design (Hampton, VA: NASA Langley Research Center)
[7] Drela M and Youngren H, 2004. *Athena Vortex Lattice.* Massachussets Institute of Technology.
[8] Gudmundsson S, 2013. *General Aviation Aircraft Design*. (Butterworth-Heinemann).
[9] Roskam J, 1985. *Airplane Design Part VI: Preliminary Calculation of Aerodynamic, Thrust and Power Characteristics.* (DARCorporation).
[10] Drela M, 2000. *xFoil.* Massachussets Institute of Technology.
[11] www.openvsp.org, 2012. *VSPAero.* Under NASA Open Source Agreement v.1.3.
[12] Patterson M D, 2016. *Conceptual Design of High-Lift Propeller Systems for Small Electric Aircraft*, (Georgia: Georgia Institute of Technology). Section III and 5.1.2.
[13] Deere K A, Viken J K, Viken S A, Carter M B, Cox D, Wiese M R and Farr N, 2018. Computational Component Build-up for the X-57 Distributed Electric Propulsion Aircraft. *AIAA SciTech Forum. Kissimmee, FL.*
[14] Sinnige T, van Arnhem N, Stokkermanns T C A, Eitelberg G and Veldhuis L L M, 2019. Wingtip-Mounted Propellers: Aerodynamic Analysis of Interaction Effects and Comparison with Conventional Layout. *Journal of Aircraft* **56** No 1. Pp 295-312.
[15] Page V R, Dickinson S O and Deckert W H, 1968. Large scale wind-tunnel tests of a deflected slipstream STOL model with wing of various aspect ratios. *NASA TN D-4448.*
[16] de Vries R, Brown M and Vos R 2019 Preliminary sizing method for hybrid-electric distributed propulsion aircraft *J. of Aircraft* 6 **56** 1-17
[17] Pornet C and Isikveren A T 2015 Conceptual design of hybrid-electric transport aircraft *Progress in Aerospace Sciences* **79** 114-35
[18] Geiß I, Notter S, Strohmayer A and Fichter W 2018 Optimized operation strategies for serial hybrid-electric aircraft *Aviation Technology, Integration, and Operations Conf.*
[19] David C, Delbecq S, Defoort S, Schmollgruber P, Benard E and Pommier-Budinger Valérie 2020 From fast to fast-oad: An open source framework for rapid overall aircraft design in*10th EASN International Conference on Innovation in Aviation Space to the Satisfaction of the European Citizens*